Structural stability of ultra-high temperature refractory material $MoSi_2$ and Mo_5Si_3 under high pressure*

Hao Liang(梁浩)[1], Fang Peng(彭放)[1,†], Cong Fan(樊聪)[1], Qiang Zhang(张强)[1], Jing Liu(刘景)[2], and Shi-Xue Guan(管诗雪)[1]

[1] *Institute of Atomic and Molecular Physics, Sichuan University, Chengdu* 610065, *China*
[2] *Institute of High Energy Physics, Chinese Academy of Sciences, Beijing* 100049, *China*

(Received 21 December 2016; revised manuscript received 17 February 2017; published online 6 April 2017)

In-situ angle dispersive x-ray diffraction (ADXRD) with synchrotron radiation source is performed on an ultra-high temperature refractory of $MoSi_2$ and Mo_5Si_3 by using a diamond anvil cell (DAC) at room temperature. While the pressure-induced volume reduction is almost constant, the value of the bulk modulus increases with the decrease of molybdenum content in the system. According to the Brich–Murnaghan equation, the bulk modulus 222.1 (2.1) GPa with its pressure derivative 4 of $MoSi_2$, and the bulk modulus 308.4 (7.6) GPa with its pressure derivative 0.7 (0.1) of Mo_5Si_3 are obtained. The experimental data show that $MoSi_2$ has distinct anisotropic behavior, Mo_5Si_3 is less anisotropic than $MoSi_2$. The result shows that $MoSi_2$ and Mo_5Si_3 have the structural stabilities under high pressure. When the pressure reaches up to 41.1 GPa, they can still maintain their body-cantered tetragonal structures.

Keywords: high pressure x-ray diffraction, molybdenum silicide, synchrotron radiation, bulk modulus

PACS: 31.15.ae, 61.05.cp, 62.20.−x **DOI:** 10.1088/1674-1056/26/5/053101

1. Introduction

High-temperature structural applications require material with a high melting point, high strength, superior oxidation resistance, and excellent creep behavior at elevated temperatures. This was demonstrated in a number of studies that showed that refractory metal silicide appears to be more attractive because of their superior physical and chemical properties. Nickel aluminides, titanium aluminides, and transition metal disilicides have been intensively investigated.[1–3] Refractory transition-metal silicide has been amply investigated so far, which can effectively improve the performance, such as the gas turbine engine in a power generation system:[4] even a minor increase in the efficiency of an engine can result in a significant decrease in fuel cost and reduction in harmful emissions.[5] Among the refractory metal silicides, the silicide in the Mo–Si system shows a promising potential because Mo has a lower density than other refractory metals, and Mo does not embrittle with the increases of oxygen and nitrogen contamination. In the Mo–Si system, there are three intermetallic phases, i.e., $C11_b$-structured $MoSi_2$, $D8_m$–structured Mo_5Si_3, and A15-structured Mo_3Si. The $MoSi_2$ and Mo_5Si_3 have been studied extensively in the last several decades as promising ultra-high structural materials because of their high melting temperatures (2303 K, 2018 K), relatively low densities (6.24 g/cm^3, 8.19 g/cm^3), high thermal conductivities, thermodynamic compatibilities, excellent oxidation resistances at high temperatures, and low temperature plastic deformabilities.[6,7] However, each of $MoSi_2$ and Mo_5Si_3 exhibits the phenomena of poor fracture toughness, poor creep strength at high temperatures, and accelerating oxidation in 450 °C–550 °C, so that there are great difficulties with industrial applications. In order to remedy these drawbacks, extensive efforts have been made to form composite $MoSi_2$-based alloys. $MoSi_2$ is a brittle intermetallic and silicide ceramic with significant potential as the matrix phase of advanced high temperature structural composites. Meyer *et al.*[8] suggested that the Mo_5Si_3 controls the creep rate of the Si–Mo system. Recent study confirmed that the eutectic $MoSi_2$ and Mo_5Si_3 composite can significantly modify the creep strength of the $MoSi_2$.[9,10] Binary compound of silicon and molybdenum is the second nickel-based super alloy of a new class of highly competitive high-temperature structural materials, so they were widely used in $MoSi_2$-based, Mo_5Si_3-based alloys.[11,12]

It has been reported that $MoSi_2$ has a body-centered-tetragonal $C11_b$ structure of the space group $I4/mmm$ (139). There is a strong covalent bond between Si atoms aligned along the c-axis in $MoSi_2$. Mo_5Si_3 belongs to the space group $I4/mcm$ (140) with a body-centered tetragonal lattice (tI32).[13] The bulk modulus is an important engineering design parameter for material. In 1990, the elastic constant of $MoSi_2$ was calculated from the velocity of ultrasonic waves which was measured by using a simple pulse-echo method by Morihiko *et al.*[14] The bulk modulus B_0 of polycrystalline ma-

*Project supported by the Joint Fund of the National Natural Science Foundation of China and the Chinese Academy of Sciences (Grant No. U1332104).
†Corresponding author. E-mail: pengfang@scu.edu.cn
© 2017 Chinese Physical Society and IOP Publishing Ltd

terial is estimated from the following equations:

$$B_0 = \frac{1}{9}(2c_{11} + c_{33}) + \frac{2}{9}(c_{12} + 2c_{13}), \quad (1)$$

where c_{11}, c_{33}, c_{12}, c_{13}, and B_0 refer to elastic constants and isothermal bulk modulus of $MoSi_2$. The Hill approximate value of bulk modulus of Mo_5Si_3 was derived by Simmons and Wang[15] in 1971. Fu *et al.*[16] studied the phase stability, bonding mechanism, and elastic constant of Mo_5Si_3 by first-principles local-density-functional calculations in 1998. In the next year, the elastic properties of the Mo_5Si_3 single crystals were experimentally measured. The elastic modulus of Mo_5Si_3 indicates that it has less elastic anisotropy.[17] Little is known, however, about the mechanical properties under high pressure of $MoSi_2$ and Mo_5Si_3. There has been no experimental study in the behaviors of $MoSi_2$, Mo_5Si_3 in a diamond anvil cell (DAC) by using *in-situ* high-pressure angle-dispersive x-ray diffraction (ADXRD) with synchrotron radiation.

In this paper, we investigate the compression behaviors of $MoSi_2$ and Mo_5Si_3, and determine the equation of state (EOS) under high pressure. In addition, the compression behaviors of materials are analyzed mainly at pressures up to 41.1 GPa. Here, we for the first time report on the $MoSi_2$ and Mo_5Si_3 study of molybdenum silicide in DAC by using *in-situ* high-pressure ADXRD with synchrotron radiation.

2. Experimental details

The experimental samples were purchased commercially from Qinhuangdao Eno Material, of which the content of $MoSi_2$ was 98% and the rest was Mo_5Si_3. Because the strengths of $MoSi_2$ and Mo_5Si_3 are equivalent and the interaction between the specimens can be ignored under high pressure, we can analyze the compressibilities of the two samples in the same experiment. The initial materials were characterized by x-ray diffraction (XRD, model DX-2500, Dandong, China) using a Cu-$K\alpha$ radiation source with $\lambda = 1.5404$ Å to check the crystal structure, purity and morphology. Figure 1 shows the power XRD pattern of the starting specimen. In situ high pressure ADXRD measurements on powder were performed at room temperature by using a synchrotron x-ray source ($\lambda = 0.6199$ Å) of the 4W2 high-pressure station of the Beijing Synchrotron Radiation Facility (BSRF, Beijing). The DAC where there is a pair of beveled diamond anvils (300 μm culet) and the stainless steel (T301) gasket of about 45–50 μm in thickness. A 120 μm-diameter hole drilled in the center of the gasket is used as a sample chamber in this experiment. The sample was pre-compressed with a separate pair of diamond anvils and located in the hole in the gasket. Methanol-methanol mixture (4:1) was used as the pressure-transmitting medium to provide relative hydrostatic pressure. By the ruby fluorescence method, the pressure was determined during such an experiment.[18,19] The spot size of the x-ray beam was focused into a size of approximately 15×32 μm. *In-situ* powder diffraction data were recorded by using a two-dimensional (2D) imaging plate detector for further analysis. Then, the Bragg diffraction rings were converted into a series of one-dimensional (1D) intensity versus diffraction angle 2θ patterns by using the FIT2D program. It allows for detector calibration and integration of powder diffraction data scanning from the 2D detector to 1D 2θ by using a CeO_2 calibration material from NIST.[20] Finally, the diffraction patterns were indexed and refined with the GSAS program packages.

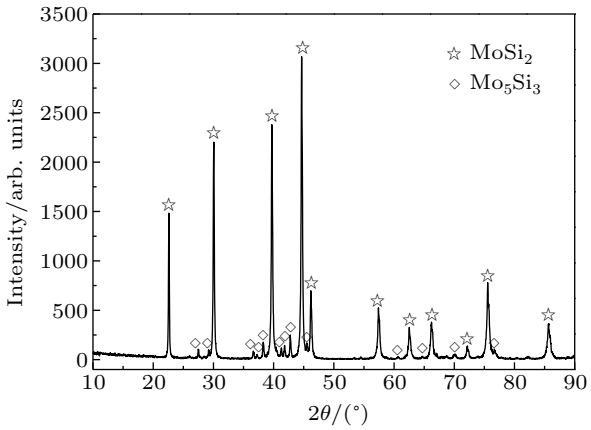


Fig. 1. The x-ray diffraction patterns of the initial specimen under normal pressure and room temperature. The five-pointed star represents the diffraction peak of $MoSi_2$ and the rhombus represents the diffraction peak of Mo_5Si_3.

3. Results and discussion

Figure 2 shows the spectrum ADXRD patterns of the initial powder under high pressure up to 41.1 GPa. From this figure we can see fifteen diffraction peaks, i.e., peaks (0 0 2), (0 1 0), (1 1 0), (1 0 3), (1 1 2), (2 0 0) for $MoSi_2$ and peaks (2 1 1), (3 1 0), (0 0 2), (4 0 0), (3 2 1), (2 0 2), (4 2 0), (4 1 1), (6 2 0) for Mo_5Si_3. Since the peak (1 1 2) for $MoSi_2$ and peaks (4 0 0), (2 0 2), (6 2 0) for Mo_5Si_3 are too low, they are not taken into account when calculating the unit cell parameters. Compared with peaks of $MoSi_2$ and Mo_5Si_3, the peak of Mo_5Si_3 is weak, but it does not affect the data analysis. With increasing pressure, all the reflections (diffraction peaks) shift toward higher 2θ angle monotonically, and become generally broadened and weakened, indicating a pressure-induced reduction of the d-spacing and thus the unit cell volume. However, these diffraction peaks are unrelated to each other in the entire compression process. These phenomena suggest that $MoSi_2$ and Mo_5Si_3 maintain their crystal structures but with reduced crystallinity. When the pressure reaches a maximum value of 41.1 GPa in this work, no new peaks are observed, so we are able to conclude that no phase transition occurs in the whole compression process.

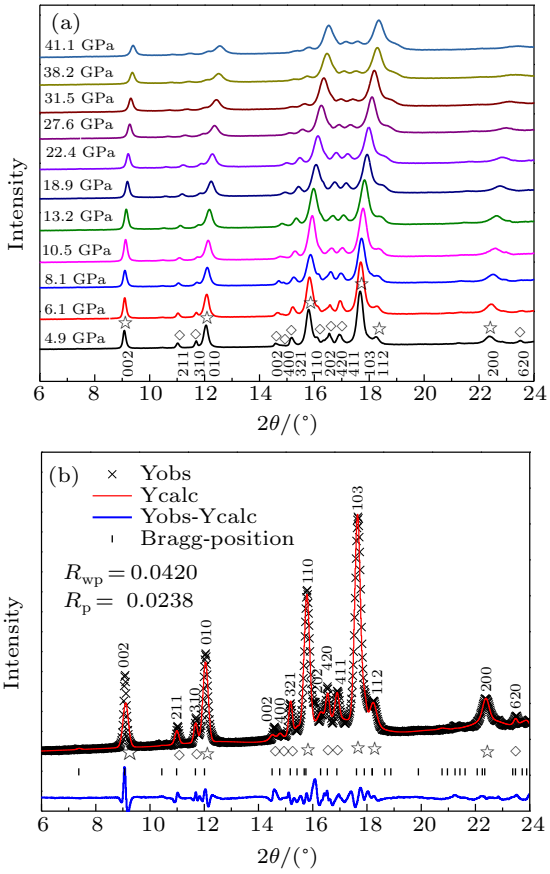


Fig. 2. (color online) X-ray diffraction patterns ($\lambda = 0.6199$ Å) of the sample under various pressures at room temperature. The five-pointed star represents the diffraction peak of $MoSi_2$ and the rhombus represents the diffraction peak of Mo_5Si_3. (a) The diffraction patterns of $MoSi_2$ and Mo_5Si_3 upon compression to the highest pressure of 41.1 GPa. (b) Rietveld refinement pattrens of the specimen about 4.9 GPa. Red line: calculated curve, black short lines: Bragg position, forks type: experimental curve, blue lines: difference curve.

Figure 3 shows the pressure evolutions of the unit-cell parameters for $MoSi_2$ and Mo_5Si_3, where the line is the fit to data. In the range of experimental error allowed, the unit-cell volume decreases with increasing pressure. The pressure-volume curves for $MoSi_2$ and Mo_5Si_3 are fitted to the best Birch–Murnaghan EOS[21,22]

$$P(V) = \frac{3}{2}B_0\left[\left(\frac{V}{V_0}\right)^{-7/3} - \left(\frac{V}{V_0}\right)^{-5/3}\right] \times\left\{1+\frac{3}{4}\left(B_0'-4\right)\left[\left(\frac{V}{V_0}\right)^{-2/3}-1\right]\right\}, \quad (2)$$

where V_0, B_0, and B_0' refer to the unit cell volume, the isothermal bulk modulus, and its first-order derivative at zero pressure for the mixed sample. The bulk modulus (B_0) and its pressure derivative (B_0') in the experiment are obtained by fixing the zero-pressure volume (V_0) at its measured value. The bulk moduli of $MoSi_2$ and Mo_5Si_3 are determined to be 222.1 (2.1) GPa, 308.4 (7.6) GPa. It has been reported that the bulk elastic modulus of $MoSi_2$ was obtained to be 209.7 GPa.[23] This indicates a relative agreement between the experimental and theoretical results. The bulk modulus of Mo_5Si_3 (242 GPa) has been derived by the Voigt, Reuss, or Hill approximation.[24] However, experimental values are slightly larger than the theoretical calculations. The theoretical calculation value is obtained by using an ideal state model. ADXRD with synchrotron radiation source is the most effective experimental method of measuring the bulk moduli of materials. As can be seen from Fig. 3, the experimental points coincide well with the fitting curve. Therefore, the experimental results are reliable and meaningful.

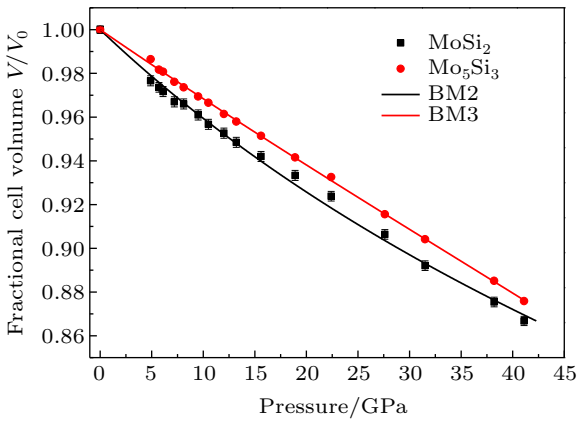


Fig. 3. (color online) Plots of normalized unit cell volume versus pressure for $MoSi_2$ (solid red circle) and Mo_5Si_3 (solid black square). The black and red solid lines represent the best fits of Birch–Murnaghan EOS.

The data listed in Table 1 are the constants for Mo, Si, $MoSi_2$, and Mo_5Si_3. It is found from Table 1 that the bulk modulus of the silicon-molybdenum compound is between the bulk moduli of Mo and Si, i.e., the bulk modulus of molybdenum (273 GPa) is the highest, and that the silicon (97.9 GPa) is the lowest. The bulk modulus of Mo_5Si_3 (308.4 (7.6) GPa) is slightly larger than the bulk modulus of $MoSi_2$ (222.1 (2.1) GPa). The discrepancies between the bulk moduli of $MoSi_2$ and Mo_5Si_3 may be explained partially by

Table 1. Values of structure parameters (a, b, c), bulk modulus (B_0), pressure derivative (B_0'), and elastic constants (C_{11}, C_{33}) of the Mo–Si system, compared with previous results of Mo, Si, Mo_5Si_3, and $MoSi_2$.

Materials	a, b/Å	c/Å	B_0/GPa	B_0'/GPa	C_{11}/GPa	C_{33}/GPa	Ref.
Mo			273				[25], [26]
Si			97.9				[27]–[29]
$MoSi_2$	3.206	7.848	210.2		417	514.5	[23]
	3.175	7.886	222.1 (2.1)	4			This work
Mo_5Si_3	9.648	4.903	242 (Hill approximation)		446	390	[24]
	9.687	4.881	308.4 (7.6)	0.7 (0.1)			This work

the fact that the differences in the structure among their crystals lead to differences in their bulk modulus. The cell volume of Mo_5Si_3 is more than 5.6 times as big as $MoSi_2$. However, the bulk modulus of $MoSi_2$ is smaller than that of Mo_5Si_3. It is well known that the interatomic bonding strength of the -Si-Mo-Si- chain is stronger than that of the -Mo-Mo- and -Si-Si- chain. In the structure of Mo_5Si_3 contained are a lot of -Si-Mo-Si- chains so that its bulk modulus is relatively high.

The compression behaviors of the unit cell axes of $MoSi_2$ and Mo_5Si_3 are shown in Fig. 4 and Table 1. We made a least-squares fitting on axis, and the fitting results yield

$MoSi_2$:

$$\frac{a}{a_0} = 1 - 1.4\times10^{-7}\left(\frac{P}{P_0}\right) + 1.3\times10^{-15}\left(\frac{P}{P_0}\right), \quad (3)$$

$$\frac{c}{c_0} = 1 - 9.9\times10^{-8}\left(\frac{P}{P_0}\right) + 6.4\times10^{-15}\left(\frac{P}{P_0}\right); \quad (4)$$

Mo_5Si_3:

$$\frac{a}{a_0} = 1 - 8.3\times10^{-8}\left(\frac{P}{P_0}\right) + 4.1\times10^{-14}\left(\frac{P}{P_0}\right), \quad (5)$$

$$\frac{c}{c_0} = 1 - 1.5\times10^{-7}\left(\frac{P}{P_0}\right) + 8.4\times10^{-14}\left(\frac{P}{P_0}\right). \quad (6)$$

Here, P_0 and V_0 are standard atmospheric pressure (1.01×10^5 Pa) and the unit cell volume under normal pressure. The results show the compressive behaviors of the a-axis and the c-axis of $MoSi_2$ and Mo_5Si_3 under high pressure. The compression curve is fitted to the highest pressure point.

Figure 4 shows the compressive behaviors in the a-axis and the c-axis directions for both materials. However, the anisotropy of $MoSi_2$ is more distinct than that of Mo_5Si_3. In general, the compressibility of the material is described by the elastic constants. The elastic constants C_{11}, C_{22}, and C_{33} represent respectively the compressibilities in the a, b, and c directions.[30] Previous studies reported that the $a\,(C_{11} = 417$ GPa) direction of the $MoSi_2$ is easier to compress than the $c\,(C_{33} = 514.5$ GPa), and the compressibilities of Mo_5Si_3 and $MoSi_2$ are just opposite, its compressibility in the $c\,(C_{11} = 446$ GPa) direction is much stronger than the $a\,(C_{33} = 390$ GPa). For $MoSi_2$, $C_{33} > C_{11}$ with $C_{33}/C_{11} = 1.26$; however, for Mo_5Si_3, $C_{33} < C_{11}$ with $C_{33}/C_{11} = 0.87$.[31] It is essential to consider the crystal structures of $MoSi_2$ and Mo_5Si_3 in order to analyze the respective anisotropic behavior.

The schematic views of $MoSi_2$ (a) and Mo_5Si_3 (b) are shown in Fig. 5. The crystal structure of $MoSi_2$ can be simply described as the accumulation of Mo and Si atoms along the c-axis. The crystal structure can be described simply as ABA′BA-type structure as shown in Fig. 5(a). In the B (silicon atoms) layer, the Si atoms of the $MoSi_2$ material are not only arranged on the a–b plane, but also form an angle with respect to the a–b plane; thus, the specially puckered B layers structure may enhance incompressibility in the c direction. In addition, the directional electronic repulsion between the silicon atoms and molybdenum atoms aligned along the c-axis can reduce the pressure induced compression in the c direction. However, unlike the Mo atom, the four Si atoms in the A (molybdenum atoms) layer are in the same plane and the layer has only one Si atom. Owing to the fact that the weak metallic bond between atoms of molybdenum is the significantly important framework, the compressibility along the a-axis is strengthened. Compared with the $MoSi_2$, Mo_5Si_3 has the extremely complex unit cell structure as shown in Fig. 5(b), in which a-lattice parameter is larger than c-lattice parameter and

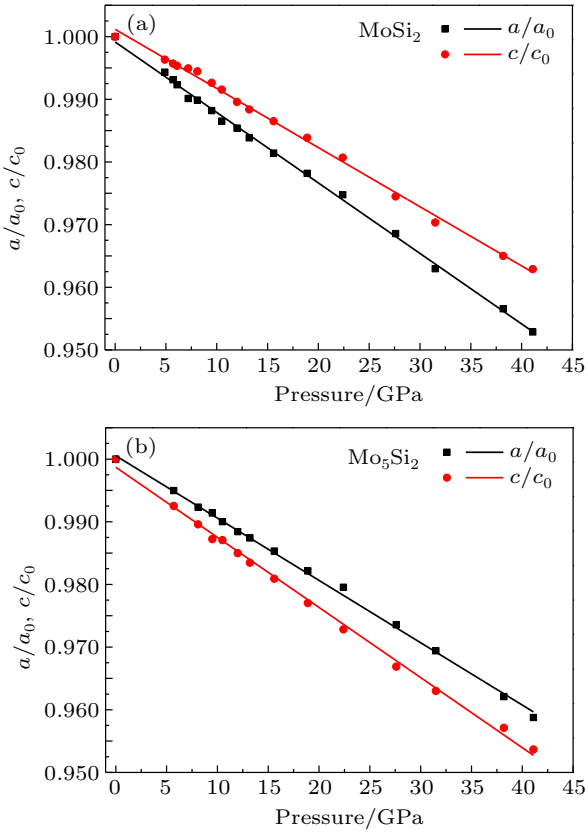


Fig. 4. (color online) Plots of cell parameter ratio (a/a_0 and c/c_0) versus pressure for $MoSi_2$ (a) and Mo_5Si_3 (b). Both a- and c-lattice constants show a gentle decrease upon compression.

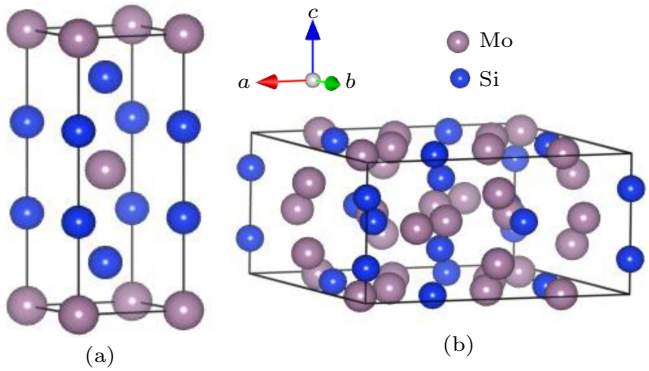


Fig. 5. (color online) Schematic crystal structures of $MoSi_2$ (a) and Mo_5Si_3 (b). Gray solid spheres represent Mo atoms and blue solid balls are Si atoms.

no close-packed planes exist. Mo and Si of atoms are alternately arranged in each unit cell. We speculate that it is this particular structure that leads to Mo_5Si_3 with less anisotropy, linear compressions in the *a*-axis and the *c*-axis almost simultaneously. However, the *a*-axis is more likely to be compressed from the overall point of view.

4. Conclusions

In this work, the structural stabilities and compressive behaviors of $MoSi_2$ and Mo_5Si_3 materials under static compression are studied by using a synchrotron radiation ADXRD technique in a DAC for the first time. $MoSi_2$ and Mo_5Si_3 are found to have a stable tetragonal structure with a maximum pressure of 41.1 GPa. The third-order Birch–Murnaghan equation is used to obtain $MoSi_2$ and Mo_5Si_3 of the bulk modulus B_0 values of 222.1 (2.1) GPa, 308.4 (7.6) GPa and the values of their pressure derivative B_0' of 4 and 0.7 (0.1). As the pressure increases, the unit cell volumes of $MoSi_2$ and Mo_5Si_3 are gradually reduced. The $MoSi_2$ *c*-axis compression rate is significantly smaller than the *a*-axis, but for Mo_5Si_3 the *a*-axis is less than *c*-axis, which reveals the anisotropies of both materials are determined by the structure of the material itself. Our study thus contributes to the design of new high temperature refractory composite materials through providing a practical guideline by considering multiple combined factors that may influence their performances in Mo–Si systems.

Acknowledgments

The high pressure ADXRD experiments were carried out at beam line 4W2 of the Beijing Synchrotron Radiation Facility (BSRF), which is supported by the Chinese Academy of Sciences (Grant No. KJCX2-SW-NO3 and KJCX2-SW-NO20).

References

[1] Darolia R, Darolia R, Lewandowski J J, Liu C T, Martin P L, Miracle D B and Nathal M V 1993 *Minerals, Metals and Materials Society* **94** 495
[2] Liu W and Dupont J N 2003 *Metall. Mater. Trans. A* **34** 2633
[3] Zhang F, Zhang L, Shan A and Wu J 2006 *Intermetallics* **14** 406
[4] Liu Y Q, Shao G and Tsakiropoulos P 2001 *Intermetallics* **9** 125
[5] Sharif A A 2010 *J. Mater. Sci.* **45** 865
[6] Berztiss D A, Cerchiara R R, Gulbransen E A, Pettit F S and Meier G H 1992 *Mater. Sci. Eng. A* **155** 165
[7] Meyer M K and Akinc M J 1996 *Am. Ceram. Soc* **79** 938
[8] Meyer M K, Kramer M J and Akinca M 1996 *Intermetallics* **4** 273
[9] Mantle A L and Aspinwall D K 2001 *J. Mater. Process. Technol.* **118** 143
[10] Schneibel J H and Sekhar J A 2003 *Mater. Sci. Eng. A* **340** 204
[11] Maloy S A, Mitchell T E and Heuer A H 1995 *Acta Metall. Mater.* **43** 657
[12] Tateoki I, Toshihiro M, Hiroyuki Y and Hideki K 2002 *J. Am. Ceram. Soc.* **85** 954
[13] Harada Y, Morinaga M, Saso D, Takata M and Sakata M 1998 *Intermetallics* **6** 523
[14] Morihiko N, Syoujiro M and Toshiyuk H 1990 *J. Mater. Sci.* **25** 3309
[15] Simmons G and Wang H 1971 *Single Crystal Elastic Constants and Calculated Aggregate Properties: A Handbook* (Cambridge: The MIT Press) p. 18
[16] Fua C L, Wanga X D, Ye Y Y and Ho K M 1999 *Intermetallics* **7** 179
[17] Chu F, Thoma D J, McClellan K J and Peralta P 1999 *Mater. Sci. Eng. A* **261** 44
[18] Mao H K, Xu J and Bell P M 1986 *J. Geophys. Res.* **91** 4673
[19] Liu J 2016 *Chin. Phys. B* **25** 076106
[20] Yang S W, Peng F, Li W T, Hu Q W, Yan X Z, Le L, Li X D and He D W 2016 *Chin. Phys. B* **25** 07610
[21] Birch F 1978 *J. Geophys. Res.* **83** 1257
[22] Murnaghan F D 1944 *Natl. Acad. Sci.* **30** 244
[23] Morihiko N, Syoujiro M and Toshiyuki H 1990 *J. Mater. Sci.* **25** 3309
[24] Lothe J P and Hirth J P 1982 (New York: Wiley) p. 270
[25] Mattheiss L F and Hamann D R 1986 *Phys. Rev. B* **33** 823
[26] Alouani M, Alber, R C A and Methfessel M 1991 *Phys. Rev. B* **43** 6500
[27] Yin M T and Cohen M L 1982 *Phys. Rev. B* **26** 5668
[28] McSkimin H J 1953 *J. Appl. Phys.* **24** 988
[29] McSkimin H J and Andreatch Jr P 1963 *J. Appl. Phys.* **34** 651
[30] Liu P P, Peng F, Yin S, Liu F M, Wang Q M, Zhu X H, Wang P, Liu J and He D W 2014 *J. Appl Phys.* **115** 163502
[31] Chu F, Thoma D J, McClellan K J and Peralta P 1999 *Mater. Sci. Eng. A* **261** 44